Available online at www.sciencedirect.com
SCIENCE DIRECT®
Combustion and Flame 146 (2006) 109–130
Combustion and Flame
www.elsevier.com/locate/combustflame

Comparative study of micromixing models in transported scalar PDF simulations of turbulent nonpremixed bluff body flames

Bart Merci [a,*], Dirk Roekaerts [b], Bertrand Naud [c], Stephen B. Pope [d]

[a] *Department of Flow, Heat and Combustion Mechanics, Ghent University—UGent, Ghent, Belgium*
[b] *Department of Multi-Scale Physics, Delft University of Technology, Delft, The Netherlands*
[c] *CIEMAT, Madrid, Spain*
[d] *Mechanical and Aerospace Engineering, Cornell University, Ithaca, NY, USA*

Received 16 November 2005; received in revised form 13 March 2006; accepted 11 April 2006

Available online 30 May 2006

Abstract

Numerical simulation results are presented for turbulent jet diffusion flames with various levels of turbulence–chemistry interaction, stabilized behind a bluff body (Sydney Flames HM1–3). Interaction between turbulence and combustion is modeled with the transported joint-scalar PDF approach. The mass density function transport equation is solved in a Lagrangian manner. A second-moment-closure turbulence model is applied to obtain accurate mean flow and turbulent mixing fields. The behavior of two micromixing models is discussed: the Euclidean minimum spanning tree model and the modified Curl coalescence dispersion model. The impact of the micromixing model choice on the results in physical space is small, although some influence becomes visible as the amount of local extinction increases. Scatter plots and profiles of conditional means and variances of thermochemical quantities, conditioned on the mixture fraction, are discussed both within and downstream of the recirculation region. A distinction is made between local extinction and incomplete combustion, based on the CO species mass fraction. The differences in qualitative behavior between the micromixing models are explained and quantitative comparison to experimental data is made.

Keywords: Numerical simulations; Nonpremixed bluff body flames HM1–HM3; Transported scalar PDF; Micromixing models (CD, EMST)

1. Introduction

With increasing computer power the transported PDF methodology, introduced by Pope [1] to model turbulence–chemistry interactions in numerical simulations of turbulent nonpremixed flames, becomes more and more tractable. In the present paper, this method is applied to turbulent jet diffusion flames that are stabilized behind a bluff body: the Sydney bluff body flames HM1–3. These flames have been target flames in the international series of TNF workshops [2] and are very well documented [2–4]. The

* Corresponding author. Fax: +32 9 264 35 75.
E-mail address: bart.merci@ugent.be (B. Merci).

0010-2180/$ – see front matter
doi:10.1016/j.combustflame.2006.04.010

Nomenclature

D	diameter (m)
k	turbulent kinetic energy (m^2/s^2)
N	number
Sc	Schmidt number
T	temperature (K)
u^+	dimensionless velocity, U/U_τ (–)
U	mean axial velocity component (m/s)
U_τ	wall stress velocity, $\sqrt{\tau_w/\rho}$ (m/s)
V	mean radial velocity component (m/s)
W	molecular weight (kg/mol)
y	normal distance from nearest solid boundary (m)
y^+	dimensionless normal distance from nearest solid boundary, $y\rho U_\tau/\mu$ (–)
Y	species mass fraction (–)
Z	total element mass fraction (–)
Γ	diffusivity (Pa s)
ε	turbulent dissipation rate (m^2/s^3)
μ	dynamic viscosity (Pa s)
ξ	mixture fraction (–)
ρ	density (kg/m^3)
τ	time (s)/stress (Pa)
ψ	composition sample space vector

Subscripts

b	bluff body
c	convection
cf	co-flow
d	diffusion
w	wall
C	carbon
F	fuel
H	hydrogen
O	oxygen/oxidizer
PC	particles per cell

configuration combines a complex flow and mixing field with well-defined boundary conditions so that it is appealing to modelers. There is an increasing amount of interaction between turbulence and combustion from flame HM1 to HM3, including local extinction. A more detailed description is given in the next section.

In a recent article Liu et al. [5] extensively illustrated the numerical accuracy of their results for the test case mentioned, applying the joint PDF of velocity, turbulence frequency, and composition (species mass fractions and enthalpy). In the present paper, we use similar numerical settings. A major difference from the method of [5] is that here we only include the scalar thermochemical quantities as independent variables in the PDF. Turbulence is modeled with the "modified LRR-IP" second-moment-closure model, as recommended in [6]. It is illustrated that this leads to accurate flow and turbulence fields.

The focus of the paper is on the performance of two widely used micromixing models: the CD (modified Curl's "coalescence dispersion") [7] and the EMST ("Euclidean minimum spanning tree") model [8–10]. The discussion mainly concerns scatter plots and conditional profiles (conditioned on mixture fraction).

The skeletal mechanism of [11] is applied as a chemistry model. Radiation is neglected, since this does not affect the observations in the present paper (see discussion later).

2. Test case description

2.1. Experimental setup

A central fuel jet (diameter 3.6 mm), 50% H_2 and 50% CH_4 by volume, emerges from the burner nozzle exit. Table 1 gives the bulk jet exit velocities for the three flames. As usual, flow field results will be compared to experiments with slightly different inflow conditions (HM1e and HM3e), which are also given in Table 1. The co-flow air stream, with free stream mean velocity as in Table 1, is separated from the fuel jet by the bluff body burner (outer diameter $D_b = 50$ mm). A more complete description is found in [2–4]. It is noteworthy that the planes with the experimental data are within the recirculation region and in the neck zone downstream, not in the jetlike flame further downstream. Fig. 1 visualizes the geometry, flow, and temperature fields by means of a numerical simulation result for flame HM3. This qualitative figure is analyzed quantitatively below.

2.2. Numerical setup

The simulations have been performed with Fluent, Version 6.2. In the numerical simulations, a nonuniform rectangular computational mesh containing 90×100 cells is used. These numbers are in between the values of grids B and C of [5]. In [12] a grid refinement study has been performed for flame HM1 in the framework of preassumed PDF simulations. The grid inlet plane is positioned at $x = -0.2D_b$, i.e., upstream of the nozzle exit $x = 0$, in order to simulate

Table 1
Bulk velocities of jet and co-flow in the different flames

Case	U_b (m/s)	U_{cf} (m/s)
HM1	118	40
HM2	178	40
HM3	214	40
HM1e	108	35
HM3e	195	35

the streamline curvature behind the bluff body accurately. This was not possible in [5]. As in [5], the grid extends to $x = 7.2D_b$ and, in the radial direction, from $r = 0$ to $r = 3D_b$. There are 8 cells within the fuel jet, 60 cells over the bluff body (stretching from the edges toward the middle of the bluff body), and 32 cells in the co-flow stream (stretching from the bluff body toward the outer radial grid boundary).

A fully developed central fuel jet is imposed at the inlet boundary. At the outer radial boundary and the right boundary, outflow conditions are applied (atmospheric static pressure is prescribed and zero radial and axial derivatives, respectively, are imposed). A boundary layer flow with the correct free stream velocity is applied for the co-flow air stream. At the adiabatic solid boundaries, among which is the bluff body face, the grid is such that $y^+ < 2$. Thus the low-Reynolds-number relation $u^+ = y^+$ is imposed in the neighboring cells. For the species, zero diffusive fluxes are applied.

As in [5,13], the transport equation for the mass density function is solved in a Lagrangian manner, following a large number of particles. The number of particles per cell, N_{PC}, is set to $N_{PC} = 100$, as suggested in [5]. In combination with time averaging over the latest 100 iterations to reduce statistical error, this value for N_{PC} is considered sufficiently high.

As in [5,13], the ISAT technique (in situ adaptive tabulation) [14] is applied to incorporate detailed chemistry in an efficient manner. In [5] it is argued that an error tolerance $\varepsilon_{tol} = 10^{-4}$ is sufficiently accurate for all species, except for NO, within their numerical setup for the simulations. Fig. 2 shows that the values of temperature and CO and OH mass fractions, conditional at stoichiometric conditions, do not vary much when the error tolerance is decreased down to $\varepsilon_{tol} = 2 \times 10^{-5}$. The values presented in Fig. 2 are mean values at given axial positions, obtained from the particles with mixture fraction in the interval $0.045 < \xi < 0.055$. Since this is around the stoichiometric mixture fraction value $\xi_{st} \approx 0.05$, this is the most sensitive region in composition space. Table 2 quantifies the differences for the three quantities mentioned. The relative difference is reported as

$$\delta = \frac{|\phi_{\varepsilon=10^{-4}} - \phi_{\varepsilon=2.10^{-5}}|}{\phi_{\varepsilon=2.10^{-5}}} \times 100 \qquad (1)$$

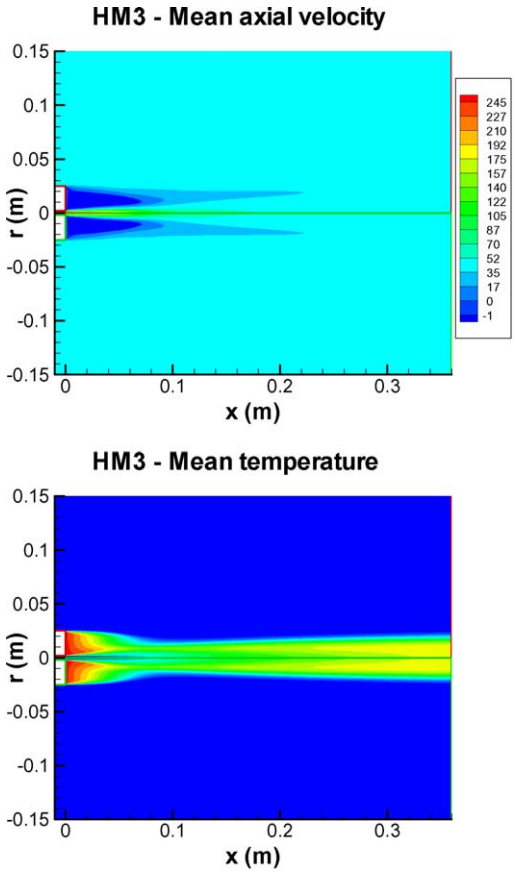

Fig. 1. Contours of mean axial velocity and mean temperature (flame HM3).

with ϕ equal to temperature or CO or NO mass fraction. Table 2 illustrates that the largest differences are observed for the minor species OH. Still, the values remain very small. The major focus of the present paper is on temperature and CO mass fraction, so that the value $\varepsilon_{tol} = 10^{-4}$ is considered sufficient, as was the case in [5]. Finally, we remark that the results in physical space are indistinguishable for the three error tolerances considered in Fig. 2 (not shown).

3. Modeling description

3.1. Turbulence modeling

The simulation results have been obtained with the modified LRR-IP Reynolds stress model, as suggested in [6]. This is the original LRR-IP model [15] for the pressure rate-of-strain term, but the value of model constant $c_{\varepsilon 1}$ in the dissipation-rate transport equation is increased from $c_{\varepsilon 1} = 1.44$ to $c_{\varepsilon 1} = 1.6$, in order to obtain better spreading-rate predictions for the round jet.

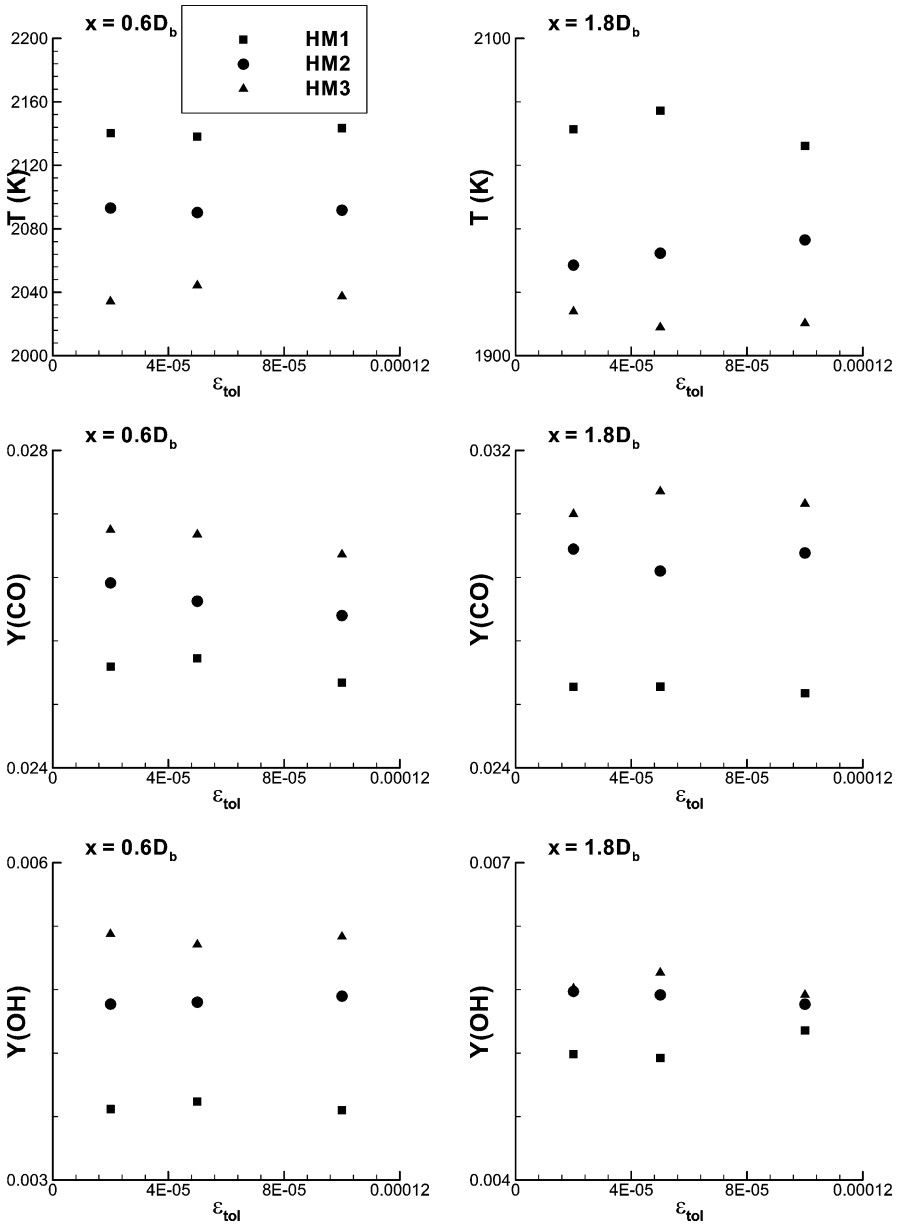

Fig. 2. Sensitivity on ISAT error tolerance of temperature and CO and OH mass fraction at stoichiometric conditions for flames HM1–3.

Table 2
Relative difference (in %) between the values with $\varepsilon_{\text{tol}} = 10^{-4}$ and $\varepsilon_{\text{tol}} = 2 \times 10^{-5}$

Position	$x = 0.6D_b$			$x = 1.8D_b$		
	HM1	HM2	HM3	HM1	HM2	HM3
T	0.2	0.1	0.2	0.5	0.8	0.4
CO	0.8	1.6	1.2	0.6	0.3	0.9
OH	0.3	1.6	0.5	4.3	2.1	1.0

There are some differences between the RSM model as applied here and the formulation in [6] with respect to the turbulent diffusion terms. The diffusion of the Reynolds stress $\widetilde{u_i'' u_j''}$ is modeled here as

$$D_{t,ij} = \frac{\partial}{\partial x_l}\left(\frac{\mu_t}{\sigma_k}\frac{\partial \widetilde{u_i'' u_j''}}{\partial x_l}\right), \tag{2}$$

instead of

$$D_{t,ij} = C_s \frac{\partial}{\partial x_l}\left(\rho \frac{k}{\varepsilon}\widetilde{u_l'' u_m''}\frac{\partial \widetilde{u_i'' u_j''}}{\partial x_m}\right).$$

Table 3
Turbulence model constants

Constant	C_1	C_2	σ_k	σ_ε	$c_{\varepsilon 1}$	$c_{\varepsilon 2}$	c_μ
Value	1.8	0.6	0.82	1.0	1.6	1.92	0.09

The eddy viscosity is defined as

$$\mu_t = c_\mu \rho \frac{k^2}{\varepsilon}. \tag{3}$$

The diffusion term in the dissipation rate transport equation is modeled as

$$D_\varepsilon = \frac{\partial}{\partial x_l}\left(\left(\mu + \frac{\mu_t}{\sigma_\varepsilon}\right)\frac{\partial \varepsilon}{\partial x_l}\right), \tag{4}$$

instead of

$$D_\varepsilon = C_\varepsilon \frac{\partial}{\partial x_l}\left(\rho \frac{k}{\varepsilon}\widetilde{u_l'' u_m''}\frac{\partial \varepsilon}{\partial x_m}\right).$$

Finally, we note that buoyancy effects are not considered. An overview of the model constants is given in Table 3. The fluent standard values are applied for σ_k and σ_ε. The influence of these model constant values on the results is expected to be small.

3.2. Chemistry modeling

As mentioned, the skeletal scheme of [11] is applied as a detailed chemistry model. It contains 31 reactions with 16 species: CH_4, O_2, H_2O, CO_2, CO, H_2, H, O, OH, HO_2, H_2O_2, CH_3, CH_3O, CH_2O, HCO, and N_2.

In [16] it is illustrated for Sandia Flames D–F [2, 17] that combustion mechanisms based on C_1 chemistry can lead to significantly greater amounts of local extinction than are observed experimentally, and they are compared to mechanisms where C_2-species are included. This deserves further research but is considered beyond the scope of the current paper.

3.3. Particle motion

As in [13], the following modeled transport equation for the mass density function $F(\psi; x, t) = \langle\rho\rangle \tilde{f}(\psi; x, t)$ is solved (with $\tilde{f}(\psi; x, t)$ the Favre PDF):

$$\frac{\partial F}{\partial t} + \frac{\partial}{\partial x_j}(\tilde{U}_j F) + \frac{\partial}{\partial \psi_k}(S_k F) = \frac{\partial}{\partial x_j}\left(\Gamma_t \frac{\partial \tilde{f}}{\partial x_j}\right) + \frac{\partial}{\partial \psi_k}\left(\left\langle \frac{1}{\rho}\frac{\partial J_{i,k}}{\partial x_i}\middle|\psi\right\rangle F\right). \tag{5}$$

As explained in [13], the equation is solved in a Lagrangian manner with local time stepping. The particles reflect at solid boundaries. In the random walk model for the turbulent diffusion term, the turbulent diffusivity is defined as $\Gamma_t = \mu_t/\mathrm{Sc}_t$. A constant turbulent Schmidt number $\mathrm{Sc}_t = 0.85$ is applied, as in [18]. We apply the standard value $C_\phi = 2.0$ for the CD model [7]. For the EMST model, the value $C_\phi = 1.5$ is recommended in [16,19]. Here we apply both values of C_ϕ with the EMST micromixing model.

4. Results for flame HM1

4.1. Results in physical space

4.1.1. Flow field results

All results reported in this section are Favre means and Favre fluctuations.

Fig. 3 shows flow field profiles for HM1 at $x = 0.2D_\mathrm{b}$, $x = 0.6D_\mathrm{b}$, $x = 1.4D_\mathrm{b}$, and $x = 1.8D_\mathrm{b}$. The experimental data, shown as filled square symbols, are for case HM1e (see Table 1). Typically (e.g., [5, 6,20–22]), flow field results are compared to these experimental data (with slightly different inlet conditions than HM1), because this data set contains measurements at more positions than for HM1. Also more than one data set is provided [2] for HM1e, so that an impression of the variability in experimental flow field data is given. We show the HM1 data, too, as open square symbols.

The primary general observation is that the differences between the profiles for the two mixing models are very small. As such, the choice of micromixing model in general does not strongly affect the mean flow field: due to the relatively small amount of local extinction for any micromixing model in the recirculation region (see next section), the mean density field remains very similar. As a consequence, the thermal expansion and, more importantly, the turbulent (shear) stresses' evolution remain practically unaffected. Some small differences between the different micromixing model profiles become visible further downstream, due to an increasing amount of local extinction with the CD model, in contrast to the EMST model (see next section). As a result, different mean density fields are predicted downstream of the recirculation region, but differences in the flow field profiles remain small.

For the Favre mean axial velocity component, overall satisfactory agreement with experimental data is obtained. Near the axis some overprediction is observed. This is due to the overprediction of mean temperature in the recirculation region (see later, Fig. 5): the central fuel jet is slowed down less rapidly due to lower values of the turbulent shear stress (which is proportional to the mean density). Indeed the near-axis overprediction was not observed in [6], where the mean temperature in the recirculation region was in better agreement with experimental data. For the dis-

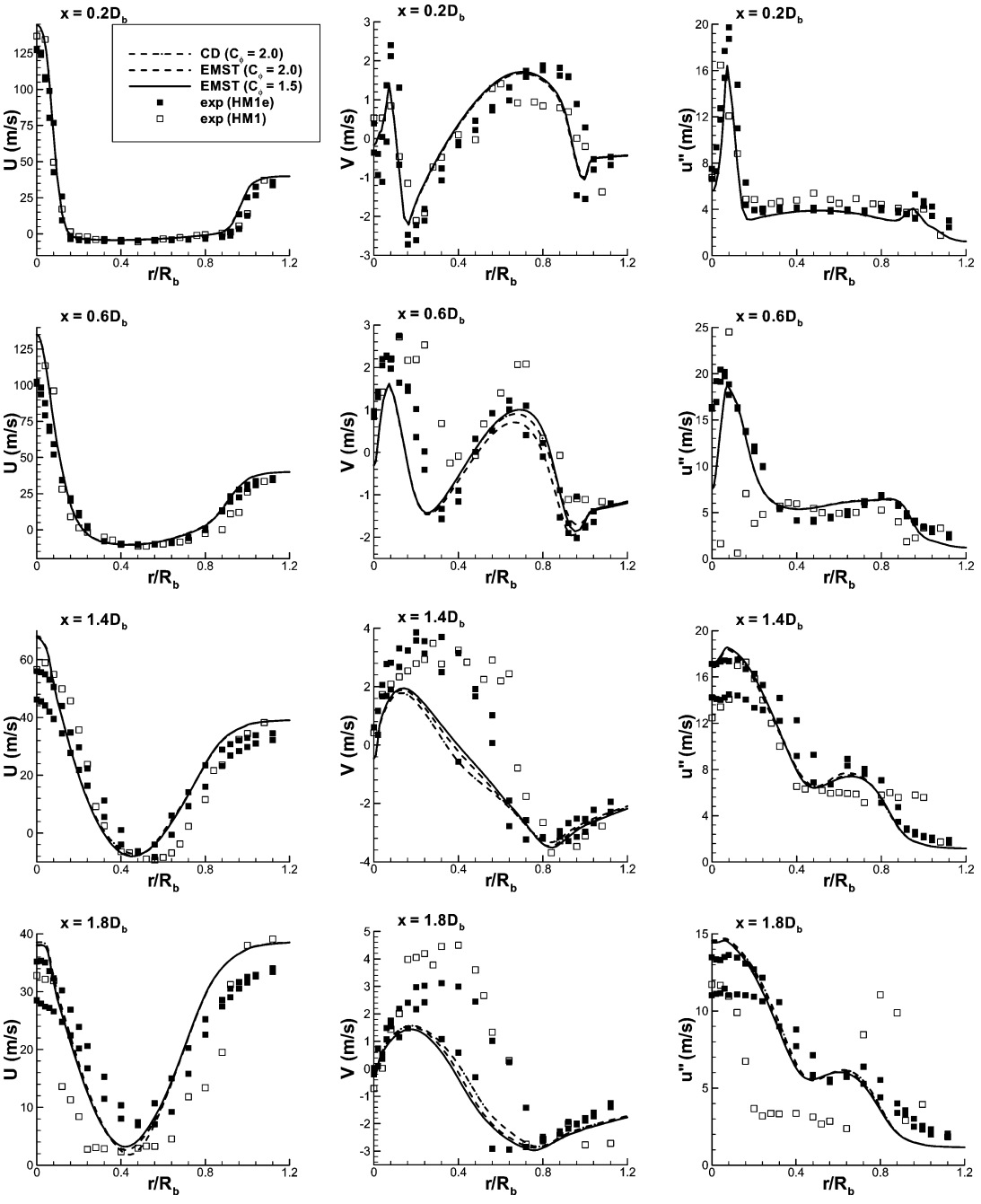

Fig. 3. Radial profiles of mean axial and radial velocity component and rms value of fluctuations (HM1).

cussion of the scatter plots and conditional profiles, which is the focus of the current paper, the near-axis overprediction is not considered a major problem, because the mixture fraction is at the rich side end, where not much happens in composition space. As such, it is by far more important that accurate mean velocity profiles and turbulent fluctuation levels are obtained in physical space where mixture fraction values are around stoichiometry in composition space. It is remarked that the recirculation region length is very well reproduced, but it is slightly too narrow, especially at the lean side. However, notable differences are observed between experimental data sets HM1 and HM1e with respect hereto.

The quality of the mean radial velocity component is considered acceptable. The general patterns are clearly followed, and note that the radial velocity component is typically much smaller than the axial component, so that the mean flow field is relatively insensitive to discrepancies in the radial velocity component.

Agreement for the velocity fluctuations is considered very reasonable, too, indicating that turbulence is accurately reproduced. Only the axial velocity fluctuations are reported here (the results for the radial velocity fluctuations are comparable). Note again the differences at $x = 1.8D_b$ between HM1 and HM1e: the simulations are in better agreement with HM1e. The double peak for u'' in HM1 is consistent with the plateau of low mean axial velocity in this data set (leading to low rms values in between the regions of high production of turbulent kinetic energy). This double peak is not captured in the simulations, is not present in the HM1e data set (neither is the plateau of low mean axial velocity), and has not been observed in recent LES simulations [20–22].

4.1.2. Scalar field results

Fig. 4 shows radial profiles for (Favre) mean mixture fraction and rms values of the mixture fraction fluctuations at $x = 0.26D_b$, $x = 0.6D_b$, $x = 1.3D_b$, and $x = 1.8D_b$. Although there are no differential diffusion effects, the mixture fraction is computed from Bilger's formula [23]:

$$\xi = \frac{\frac{2(Z_C - Z_{C,O})}{W_C} + \frac{Z_H - Z_{H,O}}{2W_H} - \frac{Z_O - Z_{O,O}}{W_O}}{\frac{2(Z_{C,F} - Z_{C,O})}{W_C} + \frac{Z_{H,F} - Z_{H,O}}{2W_H} - \frac{Z_{O,F} - Z_{O,O}}{W_O}}. \quad (6)$$

The stoichiometric mixture fraction value is $\xi_{st} \approx 0.05$.

Differences between the mean mixture fraction profiles for the EMST and the CD model are indiscernible in the figures, as could be expected from the very small differences in the flow field profiles (the mixing model choice indeed has no direct effect on the mean mixture fraction, only an indirect effect through the mean density). Due to the overestimated mean axial velocity near the axis the mean mixture fraction is overpredicted, too, in particular close to the burner. As already mentioned, this is not considered a major problem within the scope of the current paper. The mean mixture fraction profiles are in general too narrow. This is not directly related to a jet spreading rate, because the positions considered are not in the jet region.

Agreement of mixture fraction variance with experimental data in Fig. 4 is satisfactory. The peak values and the global level of rms fluctuations are very well predicted. Moreover, the shift in radial position of the rms peak value from $r = 0.1R_b$ to $r = 0.5R_b$ is reproduced. Mixture fraction variance is slightly underestimated in the recirculation region. Note that the level of velocity fluctuations is not too low (see Fig. 3), so that the underprediction of mixture fraction variance indicates that the scalar dissipation rate is too high, since the agreement for mixture fraction gradient is good. Some improvement is observed as C_ϕ is decreased to $C_\phi = 1.5$. Outside of the recirculation region, overall agreement is satisfactory (apart from some near-axis overprediction at $x = 1.3D_b$). Note that mixture fraction variance is overpredicted downstream of the recirculation region with $C_\phi = 1.5$. Finally, we also note that the results for CD and EMST with $C_\phi = 2.0$ agree, as expected.

From now on we restrict ourselves to two axial positions: $x = 0.6D_b$ (inside the recirculation region) and $x = 1.8D_b$ (downstream of the recirculation region).

Fig. 5 reveals profiles for Favre mean temperature and rms values of the temperature fluctuations. Overprediction of the mean temperature at $x = 0.6D_b$ is mainly due to the underprediction of the mean mixture fraction (so that it becomes closer to the stoichiometric value) and partly due to the neglect of radiation. Similarly, underprediction near the axis further downstream is due to overprediction of mean mixture fraction in this region (as well as due to the chemistry model, as can be seen later in the conditional mean profiles of Fig. 8 in this region of physical space and for values of mixture fraction around $\xi = 0.4$). The peak temperature at $x = 1.8D_b$ is better predicted with the EMST model (best agreement is obtained with $C_\phi = 1.5$).

The temperature fluctuation levels are in good agreement with experimental data. In the recirculation region ($x = 0.6D_b$), the underestimation of mixture fraction variance (Fig. 4), in combination with the overpredicted mean temperature, leads to correct rms values of temperature fluctuations with both mixing models for $C_\phi = 2$. With $C_\phi = 1.5$, the temperature fluctuations are somewhat overpredicted. The largest temperature fluctuations are observed at the outer radial edge of the recirculation region: a combined view with Fig. 3 reveals that the radial position of maximum rms(T'') coincides with the position where U becomes positive again. This is not surprising: turbulence production is large in this region with strong turbulent shear stresses, so that the fluctuations are strong. At the inner edge of the recirculation region, where velocities and turbulent shear stresses are even larger, this is not visible (except close to the burner, $x = 0.26D_b$, not shown), because the gas composition there is further away from stoichiometric conditions $\xi_{st} = 0.050$ (Fig. 4), so that strong mixture fraction fluctuations in this region (Fig. 4) do not lead to large temperature fluctuations. Behind the recirculation re-

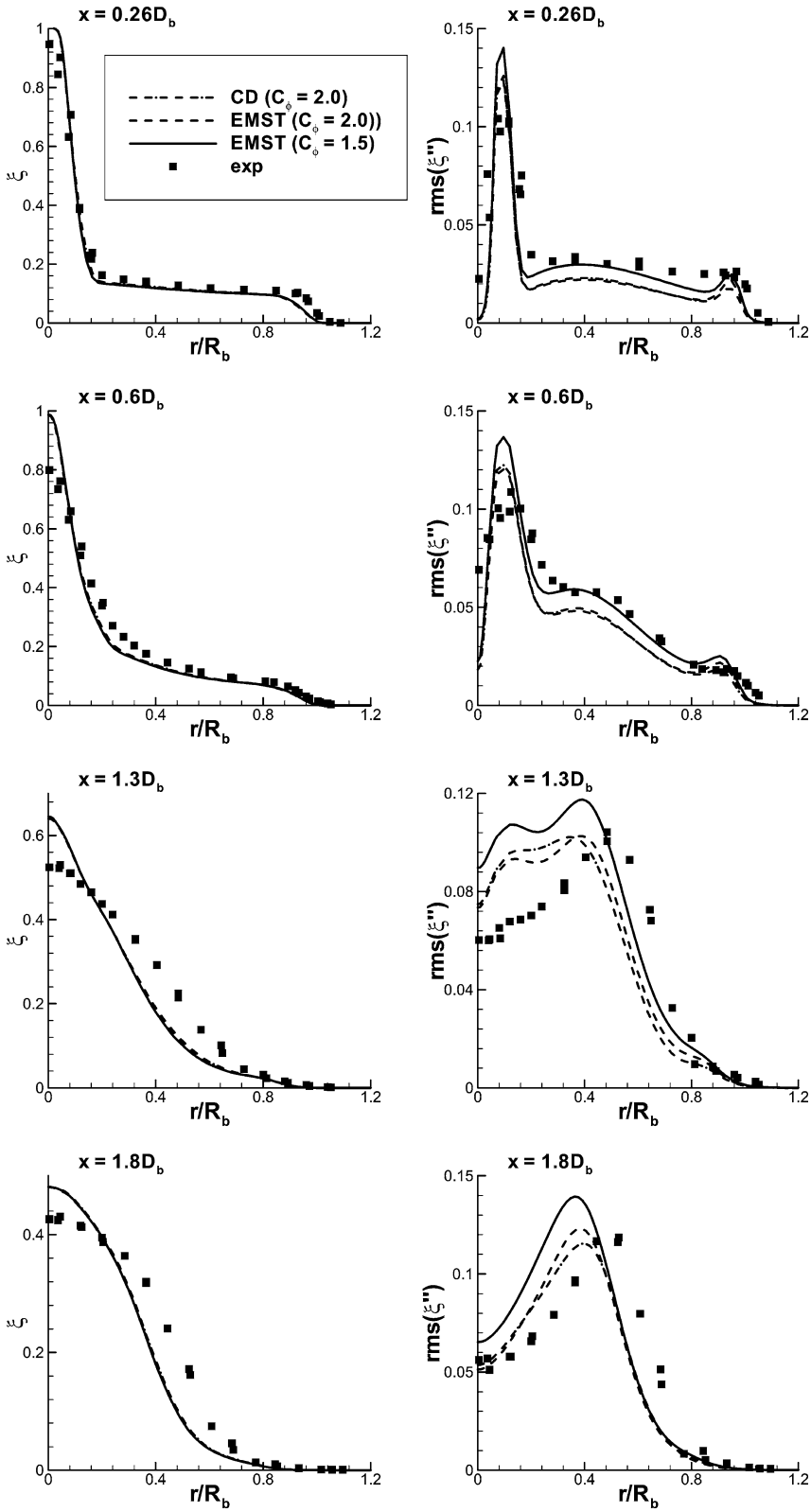

Fig. 4. Radial profiles of mean mixture fraction and rms value of mixture fraction fluctuations (HM1).

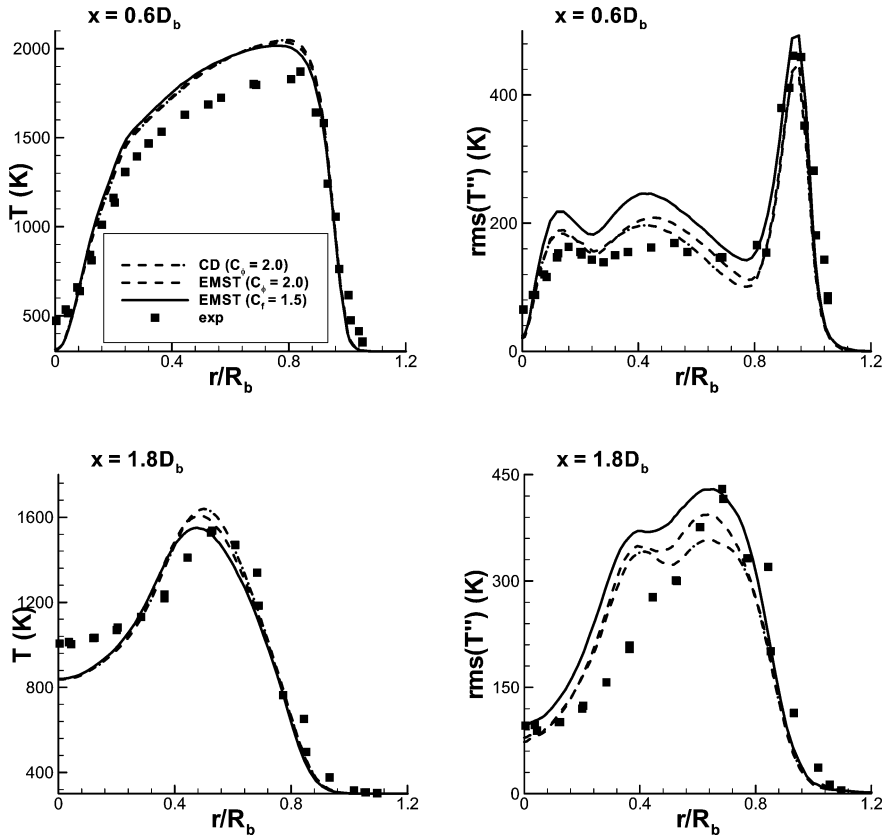

Fig. 5. Mean temperature and rms value of temperature fluctuations (HM1).

gion ($x = 1.8D_b$) the rms(T'') profile has the same shape as the mean temperature profile, indicating that the fluctuation intensity is more or less uniform. Indeed velocity gradients are less pronounced in this region.

For the major species, similar global pictures are observed (not shown).

Fig. 6 shows profiles for the minor species CO. The mean CO mass fraction is underestimated in the recirculation region. This is in line with the overestimated mean temperature and the underestimated mean mixture fraction. At the lean side of stoichiometry, there is a very strong sensitivity of the CO mass fraction value on the mixture fraction value (see, later, Fig. 9). As a result, some differences are visible. The lower values for EMST with $C_\phi = 1.5$ at $x = 0.6D_b$ are due to the slightly lower mean mixture fraction values in this zone (hardly visible in Fig. 4).

4.2. Results in composition space

The results in composition space are presented as profiles of conditional means and variances, as well as by scatter plots. For the construction of the conditional means and variances profiles, the mixture fraction interval length is 0.005. The means and variances are not weighted by density or particle numerical weights.

In the discussion of the results in mixture fraction space, the ratio of two time scales is used, shown in Fig. 7:

$$\mathrm{TR} = \frac{\min(\tau_c;\tau_d)}{C_\phi^{-1}\frac{k}{\varepsilon}} = \frac{\min\left(\frac{k^{3/2}/\varepsilon}{\sqrt{U^2+V^2}};\frac{k}{\varepsilon}\right)}{C_\phi^{-1}\frac{k}{\varepsilon}} = C_\phi \min\left(\frac{\sqrt{k}}{\sqrt{U^2+V^2}};1\right). \quad (7)$$

These time scales are obtained from the mean velocity and the turbulence length and time scales associated with the energy-containing eddies. The numerator of (7) is the minimum of a local mean convection time scale and a macroscale turbulent diffusion time scale, set equal to the local integral turbulent time scale. The denominator of (7) is the characteristic micromixing time scale, which is, as usual, assumed to be proportional to the macroscale turbulent diffusion time scale. The exact value of (7) is not as important as the correct order of magnitude for the discussion here. We describe the phenomena from a Eulerian point of

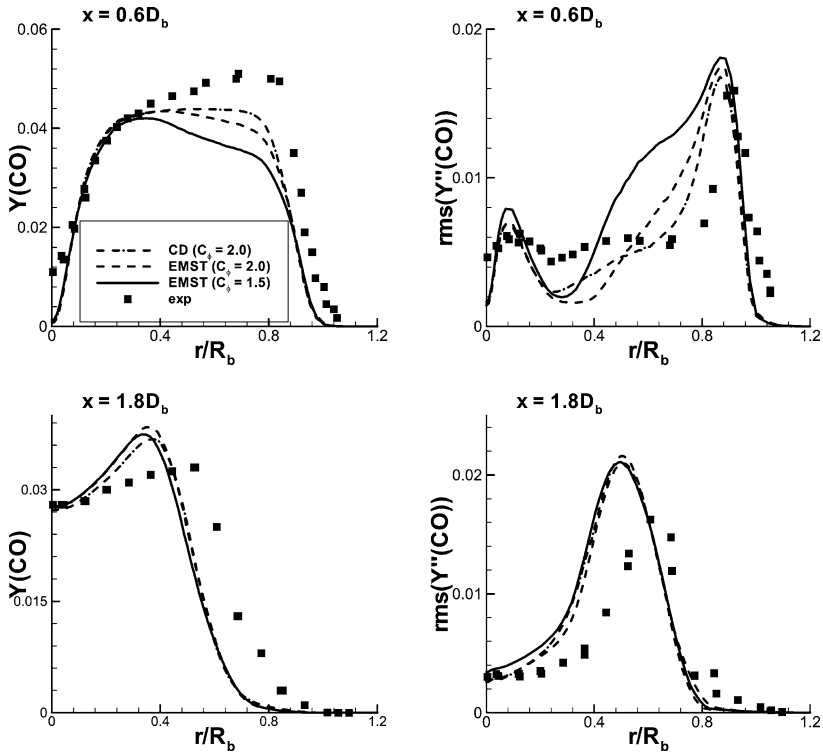

Fig. 6. Mean CO species mass fraction and rms value of fluctuations (HM1).

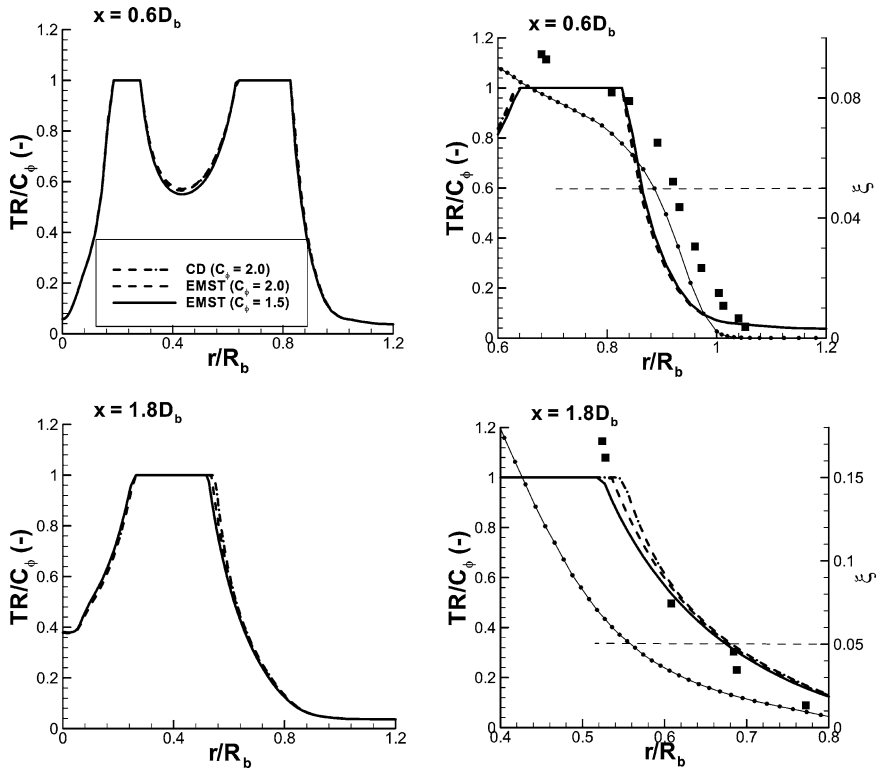

Fig. 7. Time scale ratio: particle residence time divided by mixing time (HM1).

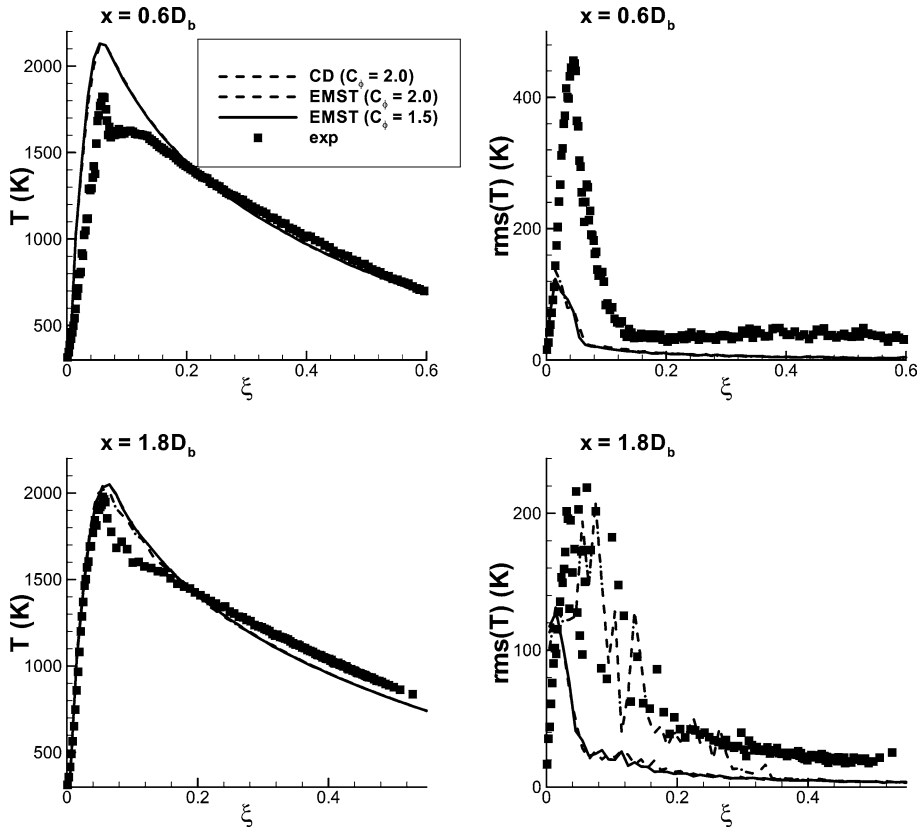

Fig. 8. Conditional means and fluctuations of temperature (HM1).

view. For sufficiently small convection time scales, the ratio (7) at a certain position expresses in a sense the time it takes for a cloud of particles to be convected by the mean flow field through an eddy in the energy containing range in the turbulence spectrum, compared to the time scale of the mixing processes taking place in the cloud of particles in the eddy. The larger the ratio (7), the more time particles receive to interact with other particles before they move out of the eddy due to mean convection.

In the left part of Fig. 7, the recirculation pattern behind the bluff body can be recognized. At the edges of the recirculation zone the convective time scale ratio in (7) reaches peak values: the mean velocities are small and at the same time the turbulent kinetic energy level is relatively large. Downstream of the recirculation region only one peak is observed, around the radial position where the mean axial velocity reaches its minimum value (Fig. 3).

The right-hand side of Fig. 7 shows the same profiles in the region where the mean mixture fraction takes values relevant for the discussion of the conditional profiles and the scatter plots, as is discussed next. The thin lines with round symbols are the simulation results for mean mixture fraction. The square symbols denote the experimental values of mean mixture fraction. A thin dashed line is drawn at the level of stoichiometric mean mixture fraction.

Fig. 8 shows conditional means and rms values of conditional fluctuations for temperature. In the conditional mean profile, a serious overprediction of temperature is observed around stoichiometric at $x = 0.6D_b$, because the high level of conditional fluctuations in the experimental data is not reproduced in the simulations. (We remark that the level of experimental conditional temperature fluctuations is much higher for flame HM1 than for HM2 or HM3; see later Figs. 14 and 18. This is due to a slight flame lift-off of HM1 in the experiments [3,4], which is not reproduced in the simulations.) As the level of conditional fluctuations decreases in the experiments further downstream, agreement improves in the simulations. In general, differences in the conditional mean profiles between the micromixing models are very small, so that we focus the discussion here on the conditional fluctuations. At $x = 0.6D_b$ it is seen in the simulation results in Fig. 7 that the mixing time scale is relatively long compared to the convective time scale when $\tilde{\xi} < 0.06$. As a result, conditional temperature fluctuations are larger for $\xi < 0.06$

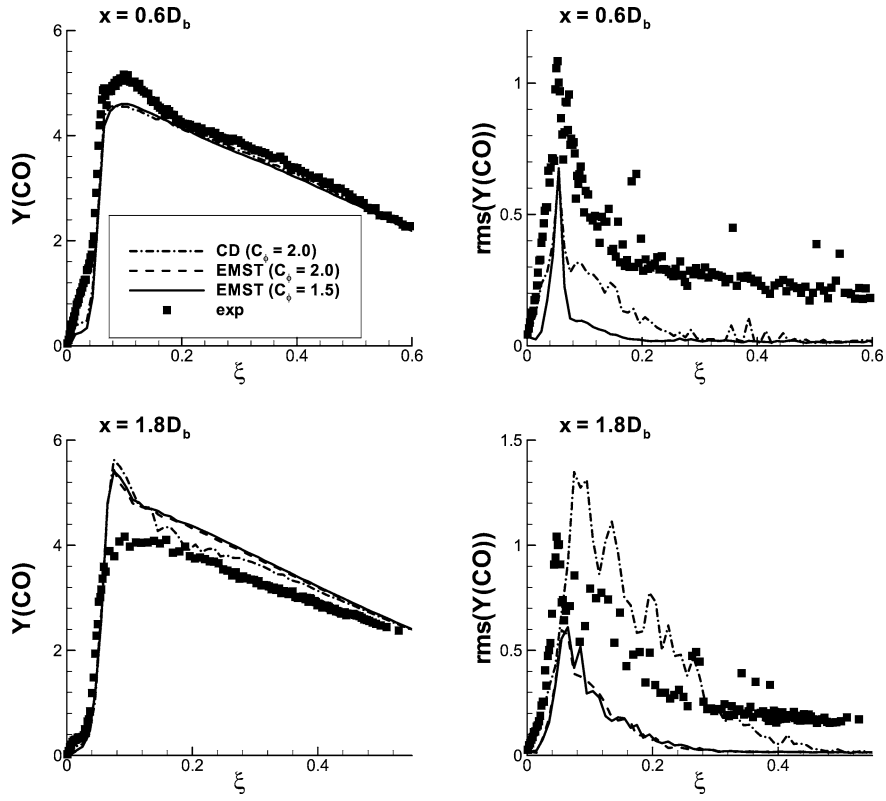

Fig. 9. Conditional means and fluctuations of CO species mass fraction (HM1).

(Fig. 8). The position of the conditional rms peak value is reached in the simulations at $\xi \approx 0.02$ with both mixing models, i.e., at the lean side of stoichiometric conditions. Note that in physical space, the particles with $\xi \approx 0.02$ are mainly around the position of maximum (unconditional) rms value of spatial temperature fluctuations (Fig. 5). In the experimental data, we see in Fig. 7 that the discussion above is shifted toward higher mixture fraction values, which is confirmed in the experimental data for conditional rms(T'') in Fig. 8. (In order not to overload the figure, no experimental data of the time scale ratio have been included in Fig. 7; keeping in mind the very good agreement for mean axial velocity and velocity fluctuations, illustrated in Fig. 3, the discussion can be held by means of the simulation results for the time scale ratio.) At $x = 1.8D_b$, a clear increase in conditional fluctuations around stoichiometry is observed with the CD model (while the level of conditional fluctuations increases at the rich side, too). With EMST this is not observed, due to the localness property: particles mainly interact with neighboring particles in mixture fraction space. The globally higher level of conditional fluctuations with the CD model is due to the intrinsic properties of the model (mixing between randomly chosen pairs of particles).

Fig. 9 shows the conditional means and fluctuations for the minor species CO. The same general observations can be made as for temperature, for the same reasons.

To conclude the discussion on the conditional profiles, we note that the influence of the value of C_ϕ is small with the EMST mixing model.

5. Results for flame HM2

No flow field measurements are available for this flame.

Fig. 10 shows profiles for mean mixture fraction and the rms value of the mixture fraction fluctuations. Agreement with experimental data is comparable to what has been achieved for HM1 (Fig. 4). Mixture fraction variance is overpredicted with $C_\phi = 1.5$.

Fig. 11 reveals some slight differences between the mixing models in the mean temperature profiles. In the recirculation region, the experimentally observed mean temperature increase toward $r = 0.8R_b$ is not well reproduced, because mean mixture fraction is slightly underestimated (Fig. 10). (Note that this phenomenon was correctly obtained in [5], but in those results mean mixture fraction was somewhat overestimated.) With EMST, the maximum of

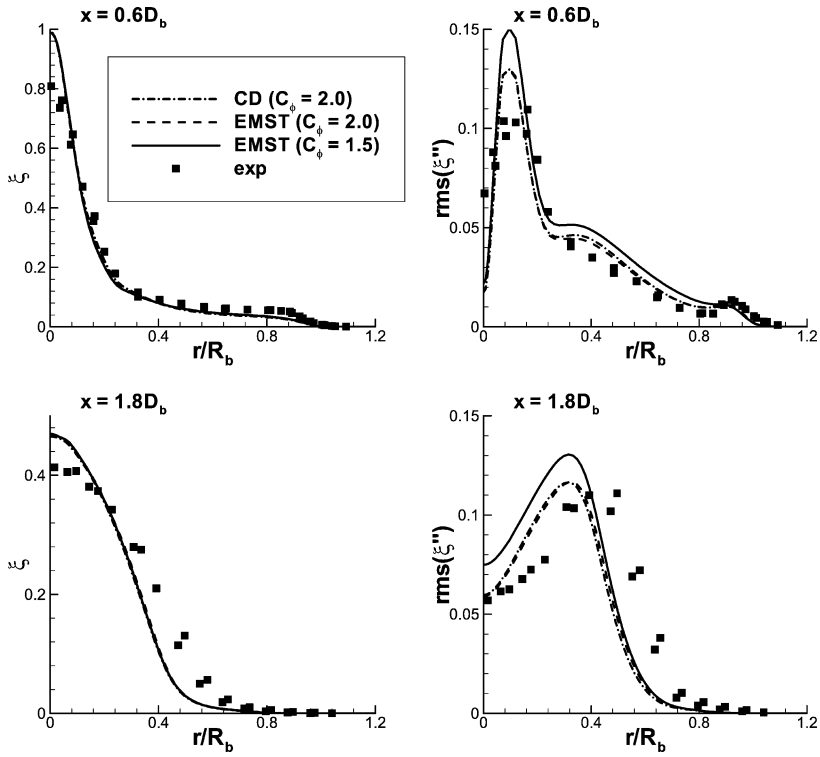

Fig. 10. Radial profiles of mean mixture fraction and rms value of mixture fraction fluctuations (HM2).

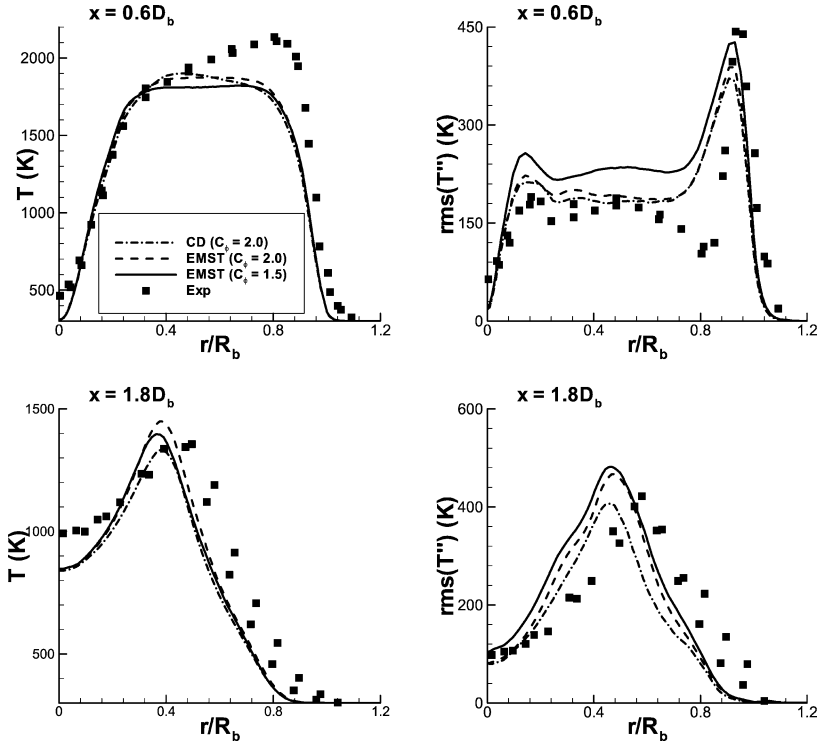

Fig. 11. Mean temperature and rms value of temperature fluctuations (HM2).

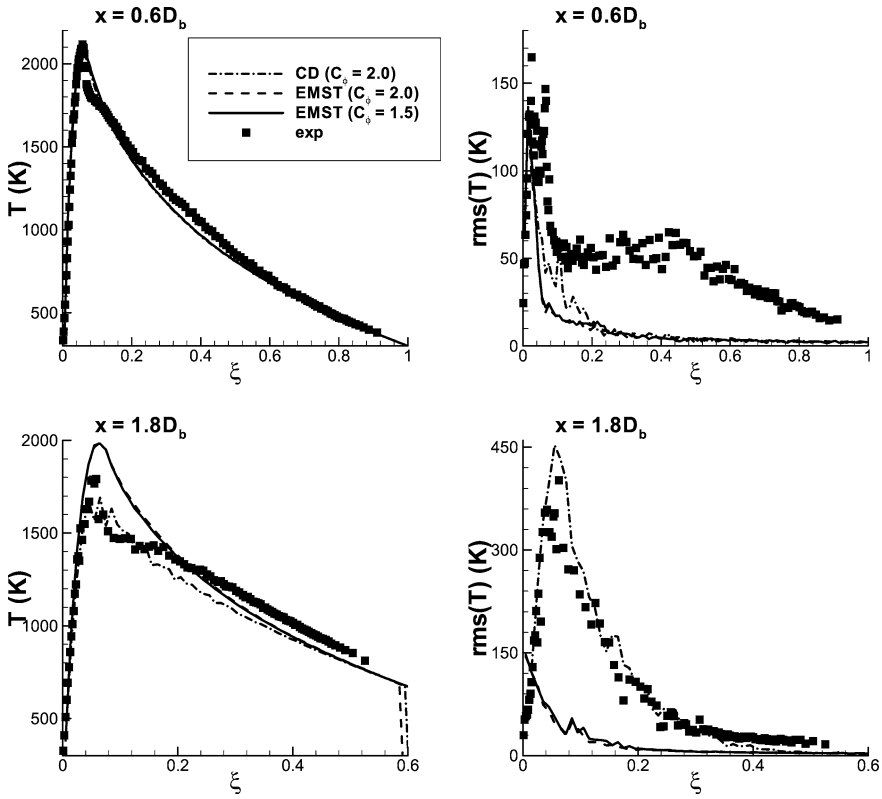

Fig. 12. Conditional means and fluctuations of temperature (HM2).

the mean temperature radial profile at $x = 0.6D_b$ is still at the outer edge of the recirculation region, in line with the experimental data. This is not the case with CD.

Despite the good agreement for mixture fraction variance (Fig. 10), the experimental dip in the temperature fluctuations around $r = 0.8R_b$ is not found in the simulations, which explains why the mean temperature is underestimated in this region. At $x = 1.8D_b$, the peak temperature value is best predicted by the CD model. Note that the CD model does not overpredict the temperature fluctuations. The reason for the better agreement with experimental data is the better agreement for the conditional temperature in this region (see Fig. 12). With EMST, the peak temperature is overpredicted at $x = 1.8D_b$, due to underprediction of local extinction (see below). Agreement improves as C_ϕ is decreased to $C_\phi = 1.5$, but at the cost of somewhat worse overprediction of temperature fluctuations. As for flame HM1, the near-axis underprediction for all models is due to mean mixture fraction overprediction.

Fig. 12 shows the conditional means and fluctuations of temperature. At $x = 0.6D_b$, agreement with experimental data for the conditional mean temperature is very good for all models. Note that agreement is better than for HM1 (Fig. 8), where the experimental conditional temperature fluctuations are much higher. With the CD model, good agreement is retained further downstream, while an overprediction of conditional mean temperature is observed around stoichiometric with the EMST model, due to underprediction of the amount of local extinction. This is seen in Fig. 13, as well as in the profiles for conditional temperature fluctuations. Very good agreement is obtained with the CD model, while the fluctuations are seriously underestimated by the EMST model. The latter is again due to the localness principle, which makes the EMST model more strongly resistant to local extinction. In Fig. 13, we indeed observe an evolution of particles toward the inert mixing limit with the CD model, in agreement with the experimental observations. With the EMST model, this is by far less pronounced. Lowering the C_ϕ-value does not remedy this.

The scatter plots for CO mass fraction, shown in Fig. 14, confirm these observations. Although further in-depth research is required, the minor species CO mass fraction seems an interesting quantity in that it may allow one to distinguish between local extinction or inert mixing (lower values of CO mass fraction) and incomplete combustion (higher values of

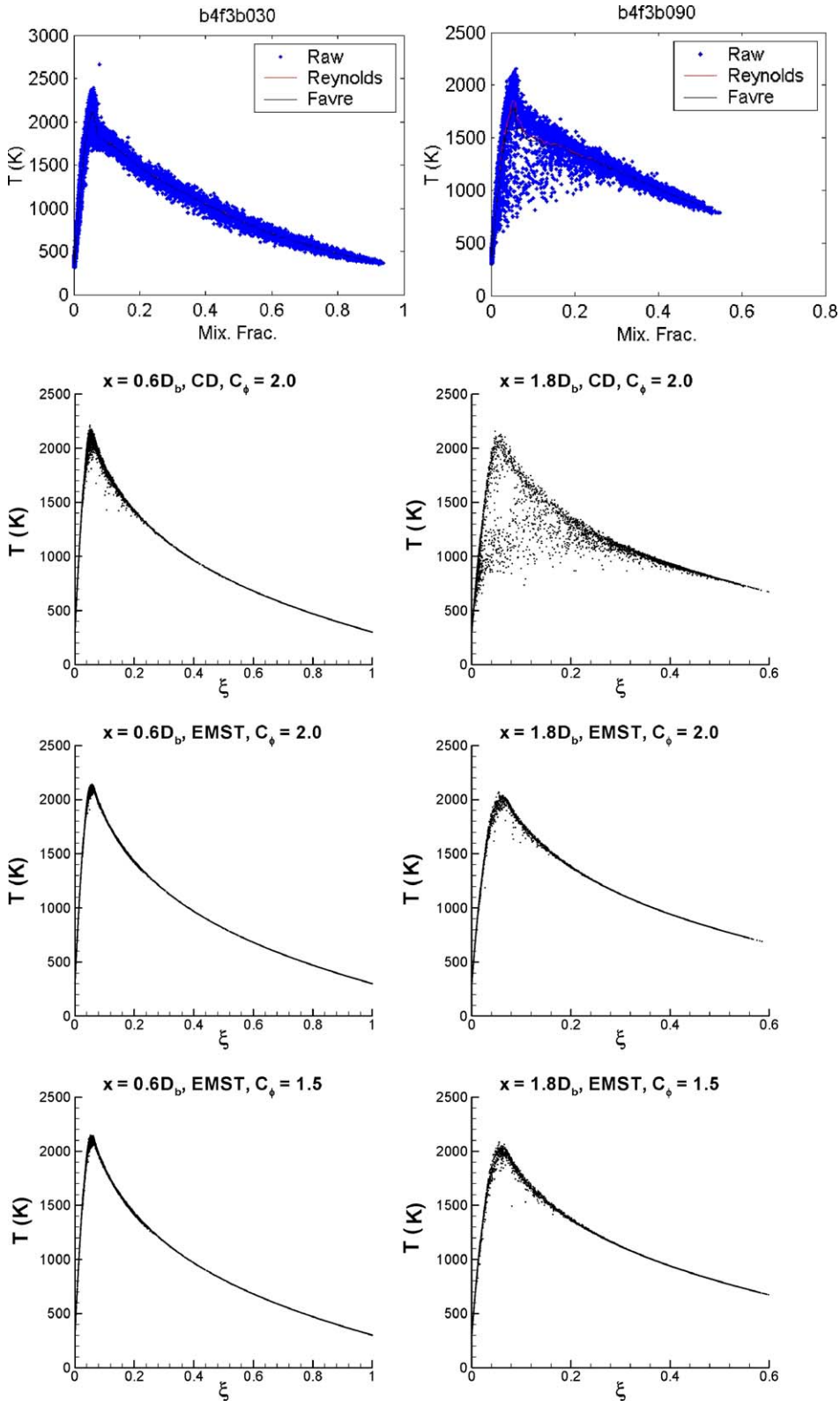

Fig. 13. Scatter plots for temperature (HM2).

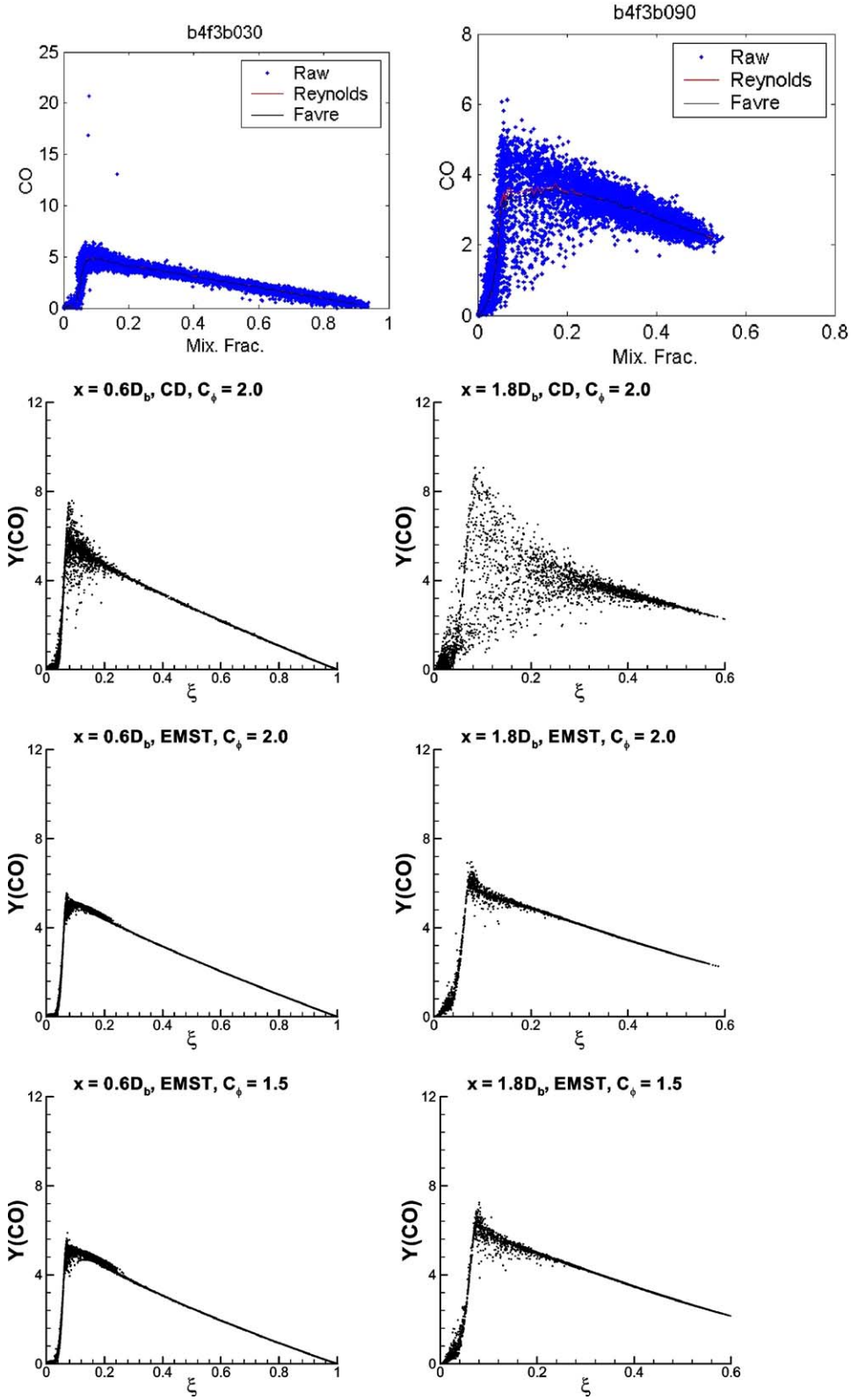

Fig. 14. Scatter plots for CO mass fraction (HM2).

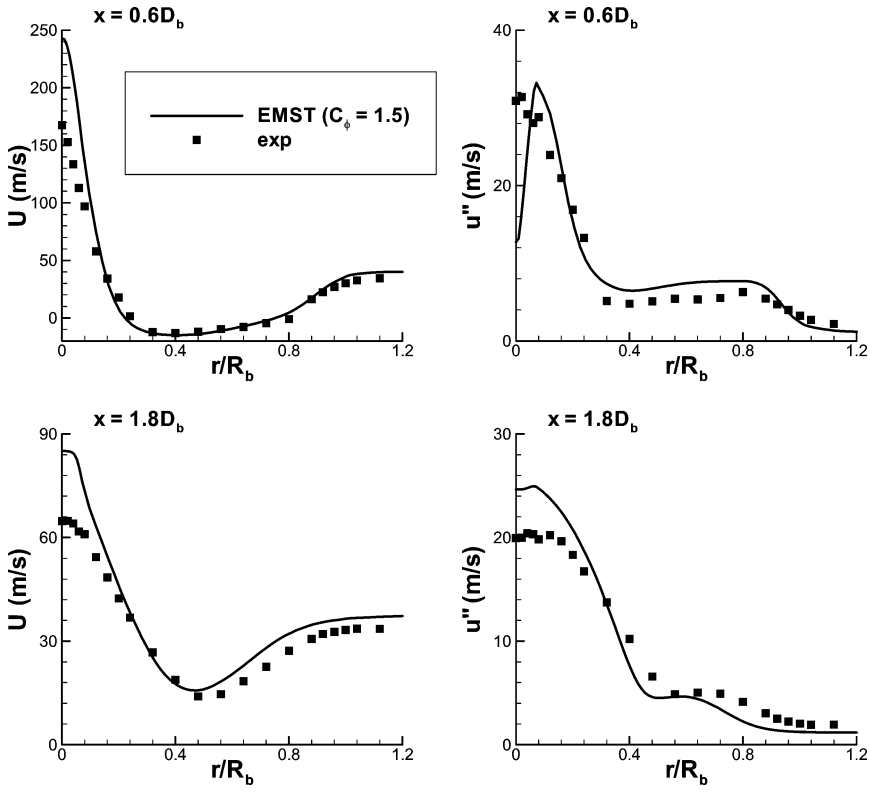

Fig. 15. Radial profiles of mean axial velocity component and rms value of fluctuations (HM3).

CO), in contrast to, e.g., temperature or H_2O (where both phenomena lead to lower values). Experimentally, relatively little local extinction is observed in the recirculation region. Behind the recirculation region more local extinction is observed in the experiments. The EMST model underestimates this local extinction, which is in line with the results discussed in [13,16]. The CD micromixing model does a better job with respect to local extinction. The price to pay seems that incomplete combustion is overestimated with this mixing model: much higher (too high) values of CO mass fraction are obtained with the CD model, in comparison to the experimental data.

6. Results for flame HM3

For flame HM3, with the strongest turbulence–chemistry interaction in the series of flames considered here, no stationary solution is obtained with the CD mixing model. The flame evolves toward global extinction, but then reignites and a limit cycle occurs. With the EMST mixing model, on the other hand, a statistically stationary flame is obtained. Therefore, we only report the EMST results for flame HM3. Differences between $C_\phi = 1.5$ and $C_\phi = 2.0$ are very small again, so that only the results with $C_\phi = 1.5$ are shown in the pictures.

As mentioned, the experimental flow field data have been gathered for slightly different inflow conditions (flame HM3e, see Table 1). Fig. 15 shows that both the mean axial velocity component and the rms value of its fluctuations are in good agreement with experimental data. The overall level of accuracy is comparable to what was obtained for flame HM1 (Fig. 3). We observe again a near-axis overprediction, but this is partly due to the higher inlet velocity for flame HM3 than with HM3e. As explained above, this overprediction is considered not dramatic for the study of the mixing model, the purpose of the present paper.

Fig. 16 confirms the good quality for the mean mixture fraction and mixture fraction variance, as was the case for HM1 (Fig. 3) and HM2 (Fig. 11). As for flames HM1 and HM2, mixture fraction variance is overpredicted in the recirculation region ($C_\phi = 1.5$).

Fig. 17 reveals that, as for flame HM2, mean temperature is underpredicted around $r = 0.8R_\mathrm{b}$ at $x = 0.6D_\mathrm{b}$. As mentioned in Section 5, this was not the case in [5], but at the cost of relatively strong overprediction of mean mixture fraction in this region. The peak temperature is now at the inner edge of the recir-

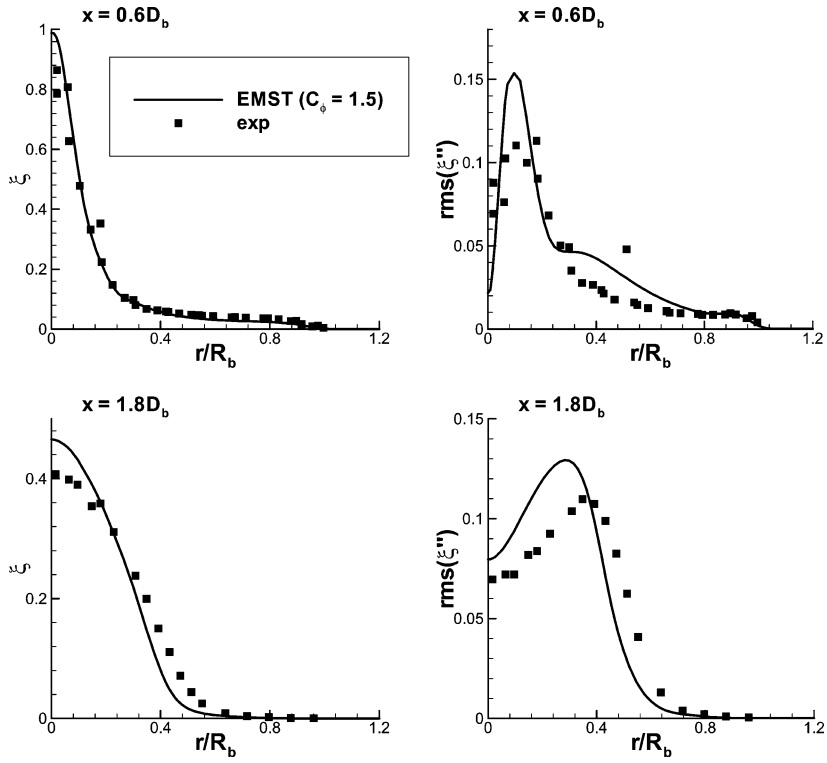

Fig. 16. Radial profiles of mean mixture fraction and rms value of mixture fraction fluctuations (HM3).

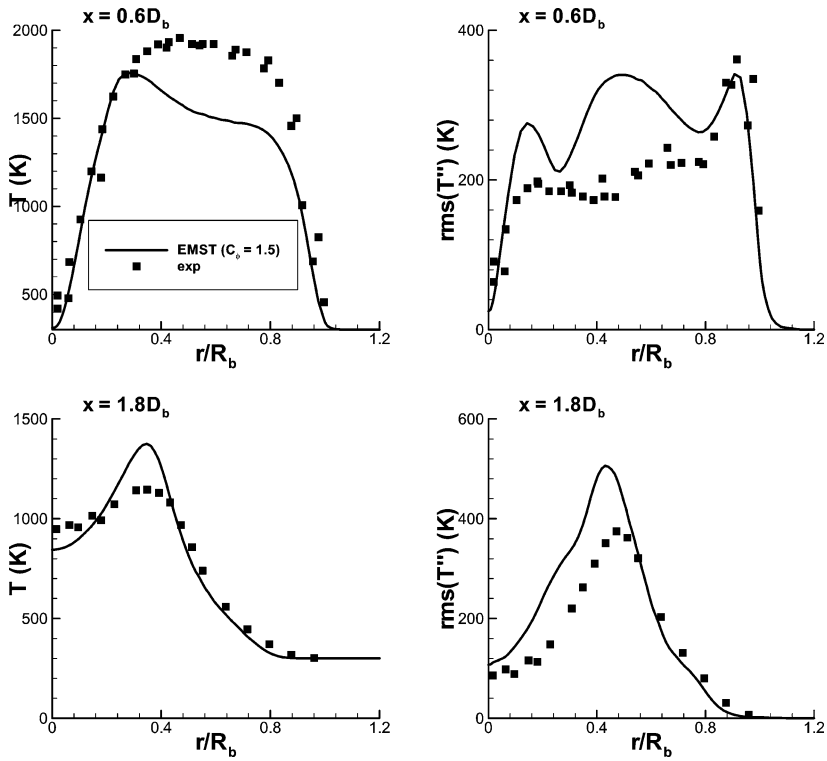

Fig. 17. Mean temperature and rms value of temperature fluctuations (HM3).

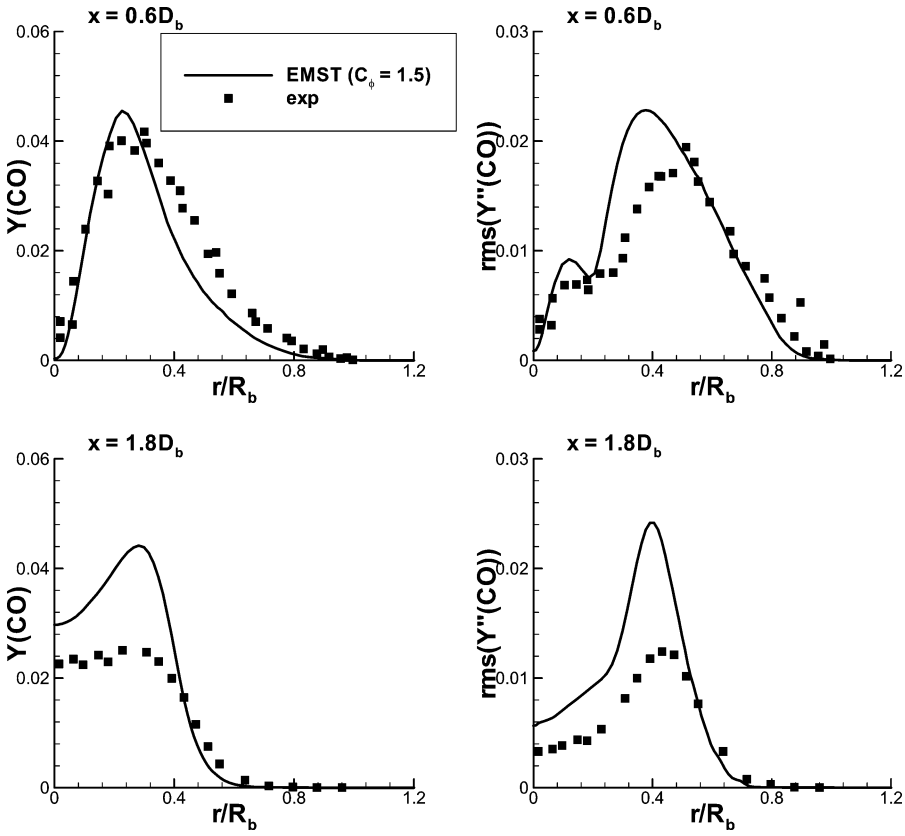

Fig. 18. Mean CO species mass fraction and rms value of fluctuations (HM3).

culation region (in contrast to flame HM2, Fig. 11). Again this is in line with the experiments for HM3, where a shift of the mean reaction zone toward the inner recirculation edge has been reported [3,4]. We also observe excessive temperature fluctuations in this zone, due to the overpredicted mixture fraction fluctuations in a region where the mean mixture fraction is close to stoichiometric (Fig. 16). At $x = 1.8D_b$, the mean temperature peak value is overestimated with the EMST model, despite overprediction of the temperature fluctuations. The near-axis underprediction is due to mean mixture fraction overprediction again.

Fig. 18 shows the profiles for CO mass fraction. Agreement with experimental data is satisfactory at $x = 0.6D_b$. The global overprediction at $x = 1.8D_b$ is probably due to the chemistry model. It is indeed well-known that C_1-chemistry schemes overpredict CO mass fractions. This is beyond the scope of the current paper.

Finally, Figs. 19 and 20 show scatter plots for temperature and CO mass fraction. In the temperature scatter plots we see, as for flame HM2, too little local extinction. As a result, the conditional mean values are overpredicted (not shown). The same is true for the CO mass fraction.

7. Discussion of the results in relation to existing literature

Since recently many journal articles have appeared on the Sydney bluff body flames, it is worthwhile to discuss some aspects of our results in this context.

In [5], the joint PDF of velocity, turbulence frequency, and composition has been applied, so that the PDF methodology is applied to model turbulence, too. Chemistry has been described by a 19-species augmented reduced mechanism, including C_2-chemistry [24]. The model constant value $C_\phi = 1.5$ is advocated. Agreement for the mean flow field is slightly better in the recirculation region, but agreement is worse near the axis from $x = 1.2D_b$ onward. This is probably due to the better agreement in [5] for mean mixture fraction and mean temperature in the recirculation region for flame HM1: mean temperature is not overpredicted, so that the central jet is slowed down more rapidly than in the current paper and underprediction of mean axial velocity is obtained downstream of the recirculation region. This is reflected in underestimated velocity fluctuations. As a result of the flow field, agreement for mean mixture fraction at $x = 1.8D_b$ is much better in the current pa-

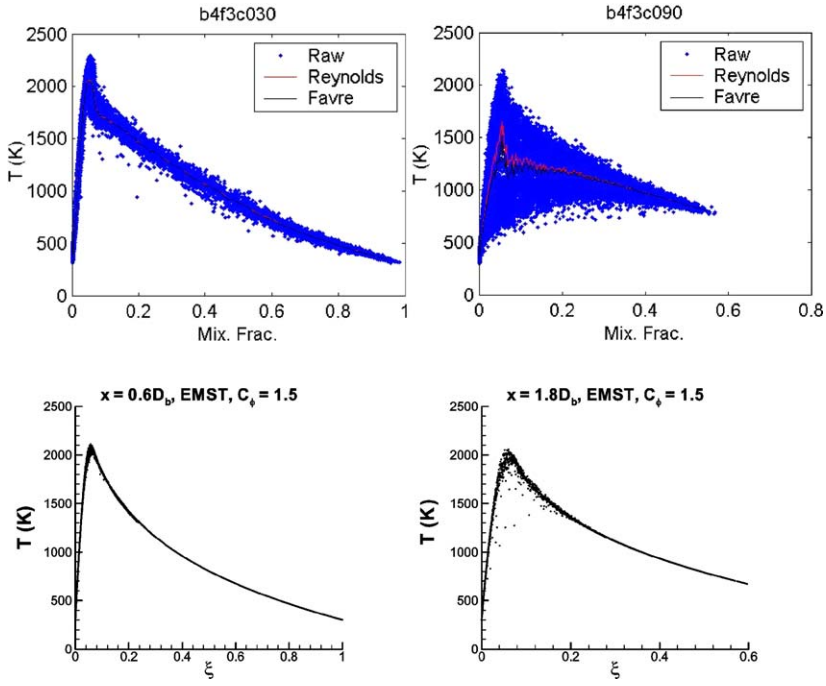

Fig. 19. Scatter plots for temperature (HM3).

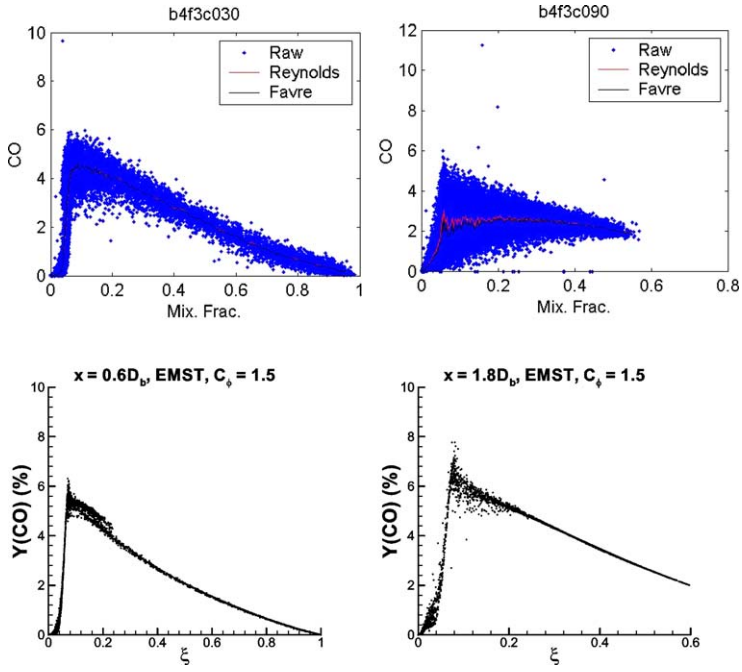

Fig. 20. Scatter plots for CO species mass fraction (HM3).

per than in [5]. The mixture fraction variance profiles are in better agreement with experimental data here, too, compared to the results in [5]. (Note that the IEM mixing model [25,26] has been applied in [5] for the profiles in physical space, but as illustrated above, the micromixing model choice hardly affects the mean turbulent mixing field in physical space, so that direct comparison to the results here can be made.) The scatter plots for temperature presented in the current paper are in very good agreement with the ones in [5],

both inside and behind the recirculation region. This illustrates the limited effect of the results in physical space on scatter plots. Here, we added CO scatter plots, too, in order to make a distinction between incomplete combustion and local extinction.

In general, the quality of the results in physical space in [5] is very similar to what had already been obtained in [27] by the same research group. The major difference between the two sets of results is the chemistry model: in [5] the detailed C_2-chemistry scheme was applied, whereas in [27] a simple flamelet/PDF technique was used. This indicates that the chemistry modeling has only a small impact on the observations for the test case under study.

In [28–30], the conditional moment closure (CMC) technique is applied. The k–ε model is applied with $c_{\varepsilon 1} = 1.6$. In physical space the quality of the results is comparable to what was presented in the current paper, with better mean temperature predictions in the recirculation region in [28]. The conditional mean profiles for temperature and CO species are practically the same in [28] and in the present paper. In [29], CMC results had already been presented with a different modification in the k–ε turbulence model. Better agreement was obtained there for mean mixture fraction and mixture fraction variance than in [28]. Still, the conditional mean profiles were very similar, which once more indicates that the quality of the turbulent mixing field in physical space and the profiles in composition space are relatively independent. This is confirmed by examining the results in [30], where the k–ε model with $c_{\varepsilon 1} = 1.6$ is applied again. The results remain very similar to [29] in general.

Finally, it is recalled that radiation has been neglected in the present study. In [31] it has been illustrated for the test case under study that inclusion of radiation hardly affects the flow and mixing field results, so that the present study is valid. The study in [31] has been performed with a modified k–ε model and a preassumed β-PDF with steady laminar flamelet modeling for chemistry (where radiation has been accounted for as a local heat loss). In general the quality of the Favre mean profiles in physical space is better in the present paper than in [31], due to application of the SMC turbulence model.

8. Conclusions

The performance of two micromixing models in the transported PDF methodology has been investigated for the case of turbulent nonpremixed turbulent jet flames, stabilized behind a bluff body.

In physical space reasonably accurate mean flow and mixing fields have been presented with a SMC turbulence model. For the unconditional means and variances of temperature, major species, and CO in physical space, there is still room for improvement, in particular for flames HM2 and HM3.

In general, the micromixing model choice has only a small influence on the results in physical space, with the important exception that no steady solution could be obtained for flame HM3 with the CD mixing model. For the other two flames, some deviations between EMST and CD become visible downstream of the recirculation region, as the amount of local extinction increases with CD, affecting the mean density field. The experimentally observed amount of local extinction is underpredicted by the EMST model. Decreasing the value of C_ϕ from 2.0 to 1.5 in general slightly improves the results, in particular for mean quantities in physical space. It also leads to a somewhat higher amount of local extinction (and thus to slightly better agreement with the experiments), but the global effect is small and fluctuations in physical space are generally overpredicted with the lower C_ϕ-value.

Starting from a comparison of the micromixing time scale to the mean convection and turbulent diffusion time scales, the observations on conditional means and variances have been explained. A low sensitivity of the EMST mixing model behavior on this time scale ratio was observed. For the CD mixing model, a much stronger sensitivity has been illustrated.

In the profiles for conditional means and variances the localness principle of EMST has been illustrated. Whereas the CD micromixing model clearly has a tendency toward uniform conditional fluctuation intensity downstream of the recirculation region, the EMST model retains the original profile shape of the conditional variances. Similarly the level of conditional fluctuations does not increase very strongly with EMST further downstream, in contrast to the CD model behavior.

It has been argued that the CO species mass fraction is an interesting quantity in that it may distinguish between local extinction (lower CO values) and incomplete combustion (higher CO values). From this observation it was derived from the scatter plots that the EMST model underpredicts local extinction, while CD yields better agreement with experimental data for flames HM1 and HM2 (no steady solution was obtained for flame HM3, as mentioned). On the other hand, CD overestimates incomplete combustion, while EMST performs well for all three flames with respect hereto.

Acknowledgments

The first author is Postdoctoral Fellow of the Fund of Scientific Research – Flanders (Belgium) (FWO-

Vlaanderen). This collaborative work has been financed by the Fund of Scientific Research – Flanders (Belgium) (FWO-Vlaanderen) through Project G. 0070.03, by the Spanish MEC under Project ENE 2005-09190-C04-04/CON, and by the Air Force Office of Scientific Research under Grant DE-FG02-90ER.

References

[1] S.B. Pope, Prog. Energy Combust. Sci. 11 (1985) 119–192.
[2] Available at http://www.ca.sandia.gov/TNF.
[3] B.B. Dally, A.R. Masri, R.S. Barlow, G.J. Fiechtner, D.F. Fletcher, Combust. Flame 114 (1998) 119–148.
[4] B.B. Dally, D.F. Fletcher, A.R. Masri, Combust. Theory Modelling 2 (1998) 193–219.
[5] K. Liu, S.B. Pope, D.A. Caughey, Combust. Flame 141 (1–2) (2005) 89–117.
[6] G. Li, B. Naud, D. Roekaerts, Flow Turb. Combust. 70 (1–4) (2003) 211–240.
[7] J. Janicka, W. Kolbe, W. Kollman, J. Non-Equil. Thermodyn. 4 (1979) 47–66.
[8] S. Subramaniam, S.B. Pope, Combust. Flame 115 (1998) 487–514.
[9] S. Subramaniam, S.B. Pope, Combust. Flame 117 (4) (1999) 732–754.
[10] Available at http://eccentric.mae.cornell.edu/~laniu/emst.
[11] M.D. Smooke, V. Giovangigli, Lect. Notes Phys. 384 (1991) 1–47.
[12] B. Merci, J. Vierendeels, E. Dick, D. Roekaerts, T.W.J. Peeters, Combust. Flame 126 (1–2) (2001) 1533–1556.
[13] B. Merci, D. Roekaerts, B. Naud, Combust. Flame 144 (3) (2006) 476–493.
[14] S.B. Pope, Combust. Theory Modelling 1 (1997) 41–63.
[15] B.E. Launder, G.J. Reece, W. Rodi, J. Fluid Mech. 68 (1975) 537–566.
[16] R.R. Cao, S.B. Pope, Combust. Flame 143 (4) (2005) 450–470.
[17] R.S. Barlow, J.H. Frank, Proc. Combust. Inst. 27 (2000) 1087–1095.
[18] B. Merci, E. Dick, C. De Langhe, Combust. Flame 131 (4) (2002) 465–468.
[19] J. Xu, S.B. Pope, Combust. Flame 123 (2000) 281–307.
[20] V. Raman, H. Pitsch, R.O. Fox, Combust. Flame 143 (1) (2005) 56–78.
[21] V. Raman, H. Pitsch, Combust. Flame 142 (4) (2005) 329–347.
[22] A. Kempf, R.P. Lindstedt, J. Janicka, Combust. Flame 144 (1–2) (2006) 170–189.
[23] R.W. Bilger, Combust. Flame 80 (1990) 135–149.
[24] C.J. Sung, C.K. Law, J.-Y. Chen, Combust. Flame 125 (2001) 906–919.
[25] J. Villermaux, J.C. Devillon, in: Proc. 2nd Int. Symp. on Chem. Reaction Eng., 1972.
[26] C. Dopazo, Phys. Fluids 18 (1975) 397–404.
[27] M. Muradoglu, K. Liu, S.B. Pope, Combust. Flame 132 (2003) 115–137.
[28] S. Sreedhara, K.Y. Huh, Combust. Flame 143 (2005) 119–134.
[29] S.H. Kim, K.Y. Huh, L. Tao, Combust. Flame 120 (1–2) (2000) 75–90.
[30] S.H. Kim, K.Y. Huh, Combust. Flame 130 (1–2) (2002) 94–111.
[31] M. Hossain, W.C. Jones, W. Malalasekera, Flow Turb. Combust. 67 (3) (2001) 217–234.